Conduction-band structure and charge-density waves in 1T-TaS_2

R. Claessen, B. Burandt, H. Carstensen, and M. Skibowski
Institut für Experimentalphysik, Universität Kiel, D-2300 Kiel 1, Federal Republic of Germany
(Received 11 October 1989)

Angle-resolved inverse photoemission spectroscopy (ARIPES) has been utilized to study the conduction-band structure of 1T-TaS_2 in the presence of charge-density waves (CDW's). In room-temperature spectra taken along the principal symmetry directions ΓM, $\Gamma M'$, and ΓK we can clearly identify Ta 5d-derived t_{2g} and e_g manifolds, which reveal a substructure of almost dispersionless peaks attributable to CDW effects. The intensity modulation of the substructure appears to reflect the band dispersion of the undistorted 1T phase. Distinct differences in intensity are observed between the ΓM and $\Gamma M'$ spectra as a consequence of the threefold symmetry of the unit cell. In temperature-dependent ARIPES between 120 and 400 K we do not, within the experimental accuracy, observe changes of the electronic structure other than a linear shift due to the electron-lattice interaction. In particular, there is no evidence of an opening of a localization gap in the unoccupied band structure as has been observed in the occupied states. From combined photoemission and inverse photoemission results the Fermi level is rather found to be pinned close to the bottom of the lowest unoccupied band.

I. INTRODUCTION

The transition-metal dichalcogenide 1T-TaS_2 has received much interest in the past few years because of the existence of several charge-density-wave (CDW) phases in this layered material. Wilson *et al.*[1,2] were the first to observe the CDW in 1T-TaS_2 directly by the occurrence of superlattice spots in electron-diffraction patterns, and they explained anomalies in the temperature-dependent resistivity by transitions between different CDW phases. Since then, several angle-resolved photoemission studies (ARPES) have been carried out on 1T-TaS_2,[3-7] not only because of the interest in the electronic structure associated with the CDW's, but also because it is an ideal test material for angle-resolved electron spectroscopies due to its distinct two-dimensional electronic structure.

In recent temperature-dependent ARPES measurements[5-7] it has been observed that upon cooling through the low-temperature phase transition at 180 K intensity is shifted from the Fermi level to higher binding energies by about 80–200 meV. This has been interpreted as the opening of a Mott-Hubbard gap due to a CDW-driven localization of the Ta 5d conduction electrons as originally suggested by Fazekas and Tosatti.[8]

In this paper we present the first angle-resolved *inverse* photoemission (ARIPES) spectra of 1T-TaS_2. The conduction-band structure of the room-temperature phase is mapped along the principal symmetry directions of the Brillouin zone up to 8 eV above the Fermi level and interpreted within the framework of existing one-electron band-structure calculations. We also performed temperature-dependent ARIPES measurements in order to study the effect of the CDW-related phase transitions on the unoccupied electronic states. Finally, from the combined knowledge about occupied and unoccupied bands, we derive a qualitative model of the temperature-dependent electronic structure around the Fermi level.

II. STRUCTURAL AND ELECTRONIC PROPERTIES OF 1T-TaS_2

In the undistorted 1T phase, TaS_2 forms a layer compound in which a sheet of hexagonally arranged metal atoms is sandwiched between sheets of sulfur atoms, with only weak bonding between successive TaS_2 sandwiches separated by "van der Waals gaps." Each Ta atom is surrounded by six sulfur atoms in octahedral coordination, which is shown in Fig. 1(a). Though the crystal structure is described by a hexagonal lattice, we have only an overall threefold symmetry due to the reduced symmetry of the unit cell. The significance of this for the band-structure and Fermi-surface properties has been emphasized by Woolley and Wexler.[9] As a consequence, we have to distinguish between the high-symmetry points M and M' in the hexagonal Brillouin zone [Fig. 1(b)], where the line $\Gamma M'$ is defined by the direction for which the sulfur atom is located in the top layer [cf. Fig. 1(a)].

The electronic structure of the 1T phase is to be described by broad bonding (σ) and antibonding (σ^*) bands formed from S 3p and Ta 6s-6p orbitals, respectively, while in the large $\sigma\sigma^*$ gap of about 8 eV we find the Ta 5d-derived conduction bands.[10] In the octahedral crystal field the 5d states split into the threefold-degenerate t_{2g} manifold and the twofold-degenerate e_g manifold. Due to a slight distortion of the perfect octahedral symmetry, the degeneracy is further lifted. There are three t_{2g} subbands formed from d_{xy}, $d_{x^2-y^2}$, and d_{z^2} orbitals, respectively, while the upper e_g manifold splits into d_{xz}- and d_{yz}-derived bands. All d bands are unoccupied except the d_{z^2}-derived one, which is half-filled and makes undistorted 1T-TaS_2 a metal.[9,11,12]

The pure 1T phase exists only in a very narrow temperature range between 543 and 570 K. Above 570 K there is an irreversible transition to the trigonal prismatic (2H) coordinated phase; below 543 K the crystal structure is

distorted by an incommensurate CDW ($1T_1$ phase). Upon further cooling, another CDW phase ($1T_2$) is reached at about 350 K, which is also present at room temperature. Finally, at about 180 K a transition occurs to a commensurate CDW ($1T_3$ phase). In the warming-up cycle the low-temperature phase remains stable up to 220 K, where a new, so-called T (triclinic) phase appears. The backtransformation to the $1T_2$ phase occurs at 280 K. The occurrence of CDW's and subsequent periodic lattice distortions (PLD's) is closely related to the two-dimensional character of the electronic structure and the possibility of Fermi-vector nesting, which can lead to divergencies in the generalized electronic susceptibility, but also electron-phonon coupling and electron-electron interaction have to be taken into account in order to provide a realistic description of CDW's.[13]

The microscopic structure of the low-temperature ($1T_3$) phase can be described by a commensurate $\sqrt{13}\times\sqrt{13}$ superlattice in the Ta layer, made up of 13-atom ("Star-of-David") clusters, which is rotated by 13.9° with respect to the underlying atomic lattice[14] [Fig. 2(a)]. The nature of the room-temperature ($1T_2$) phase has been a matter of controversy in the literature. Scruby *et al.*[15] proposed a model in which the phase is described as a nearly commensurate CDW with uniform amplitude and phase, rotated by about 12° relative to the atomic lattice at 300 K. This is the angle that has been observed in electron-diffraction studies.[2,15] In a competing model, the $1T_2$ phase consists of domains of the commensurate CDW separated by discommensurations in which the CDW phase changes rapidly.[16] Very recently, Wu and Lieber[17] found strong evidence for the commensurate domain model by scanning tunneling microscopy (STM) on cleaved $1T$-TaS_2 surfaces. They observed commensurate domains of about 70 Å in diameter, which are themselves ordered in a hexagonal array. They also found an "average" rotation angle of 11.6°±0.5° by using a vector spanning several domains to define the CDW direction. This value is close to the 12° obtained in electron diffraction, where the beam width is considerably larger than a single domain and, hence, averages over several domains.

An obvious effect of the low-temperature CDW phase on the electronic structure would be the backfolding of the bands of the undistorted $1T$ phase into the smaller CDW Brillouin zone [shown in Fig. 2(b)]. As Smith *et al.*[5] pointed out, such an umklapp procedure is not sufficient to explain the data obtained by ARPES. In an empirical tight-binding calculation taking into account

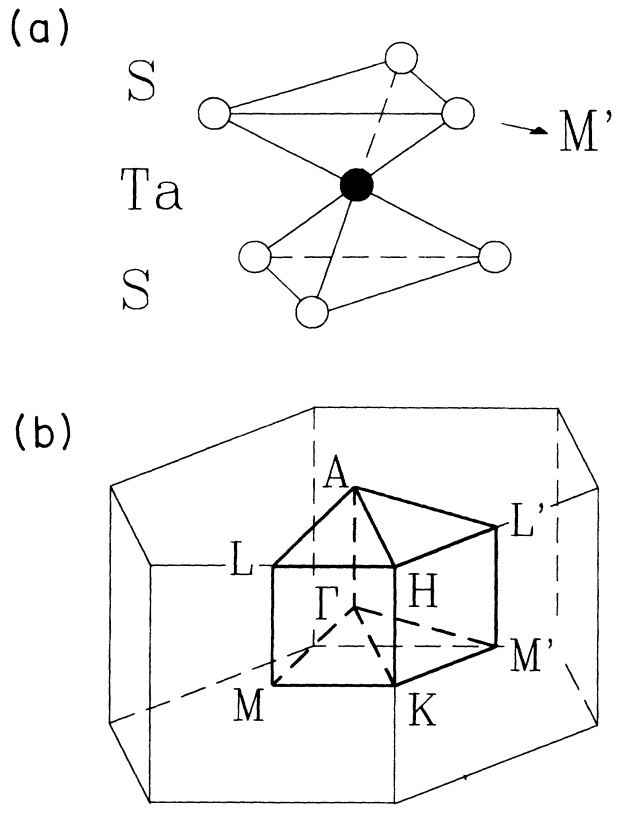

FIG. 1. (a) Unit cell of $1T$-TaS_2 showing the ocatahedral coordination of the Ta atom. (b) Brillouin zone with high-symmetry points; the line $\Gamma M'$ is defined by the direction with the sulfur atom in the top layer [see (a)].

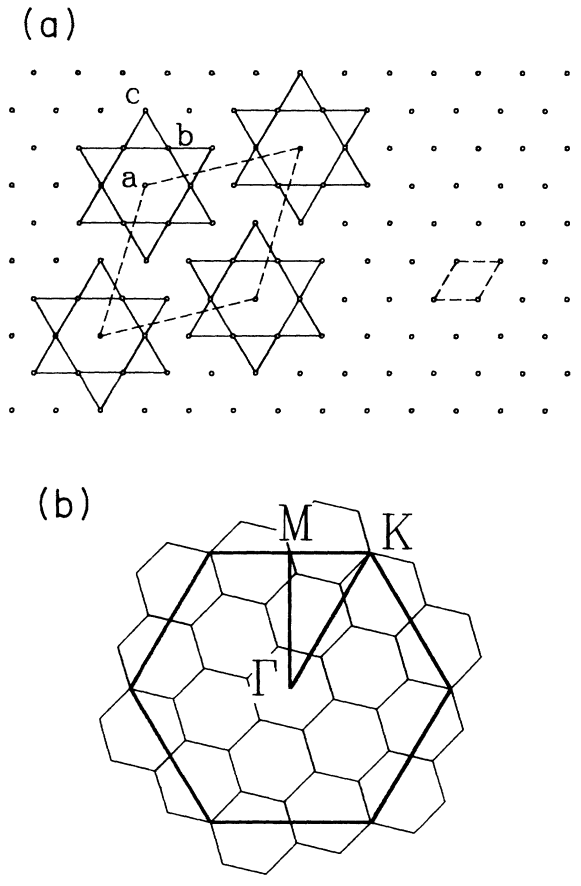

FIG. 2. (a) Right, undistorted 1×1 $1T$ structure; left, $\sqrt{13}\times\sqrt{13}$ superlattice and "Star-of-David" clusters of the commensurate CDW state; *a*, *b*, and *c* denote nonequivalent Ta atoms. (b) Basal plane of the 1×1 Brillouin zone superimposed on the $\sqrt{13}\times\sqrt{13}$ Brillouin zone.

the CDW atomic displacements, they found that in the occupied region the Ta $5d_{z^2}$– derived band decomposes into three submanifolds separated by energy gaps. The lower two manifolds consist of three individual bands each and are thus filled with six electrons each. The remaining thirteenth Ta $5d$ electron populates the upper manifold. The existence of three manifolds in the low-temperature phase has been confirmed by several ARPES studies.[4–7] Three structures have also been observed in spectra taken at room temperature, though much broader and with less intensity.[6]

Contrary to the calculation of Smith *et al.*, the upper band containing the thirteenth electron is not observed to cross the Fermi level in ARPES, but rather is shifted away from E_F by about 80–200 meV when cooling through the $1T_2$-$1T_3$ transition.[4,5,7] Fazekas and Tosatti[8] proposed a picture in which 12 of the 13 Ta d conduction electrons constitute the bonding of the 13-atom cluster, while the remaining electron becomes susceptible to a Mott localization. Thus, the CDW reconstruction drives a metal-to-semiconductor transition and the observed shift has to be interpreted as the opening of a Mott localization gap. As recently reported,[7] the gap remains observable during the warming-up cycle up to 280 K, where the retransformation from the T phase to the room-temperature phase occurs. Since this transition is related to a c-axis contraction of the crystal structure, it may be argued that also a change in the interlayer coupling contributes to the Mott localization.[7]

The aim of the present work is to investigate the effect of the CDW's on the unoccupied electronic states by means of angle-resolved inverse-photoemission spectroscopy. We are interested in changes of the conduction-band structure when going through the CDW phase transitions and, in particular, whether the opening of the localization gap can also be observed in the unoccupied region, thus determining its absolute value by combination with the photoemission results.

Because inverse photoemission, like ultraviolet photoemission, is a very surface-sensitive spectroscopy, we have to comment here on the relationship of surface and bulk properties in $1T$-TaS_2. Fortunately, since the TaS_2 sandwiches are only weakly coupled, the creation of a surface by cleaving between two sandwiches does not represent a major disturbance. Structure data obtained by bulk-sensitive transmission electron diffraction and by surface-sensitive STM are in complete agreement, and in a recent paper the cleaved surface was studied by STM while simultaneously measuring the bulk resistivity,[18] finding identical transition temperatures at the surface and in the bulk.

III. EXPERIMENT

By now, ARIPES has been well established as an experimental tool for the determination of the **k**-dependent conduction-band structure of solid surfaces.[19] In particular, the ARIPES spectrometer used in this work has already been successfully applied to study other transition-metal dichalcogenides.[20,21] It consists of a low-energy-electron source, providing an energy resolution of 220 meV [full width at half maximum (FWHM)] and a wave-vector resolution of ≈ 0.08 Å^{-1}, and a solid-state bandpass photon detector (consisting of a CaF_2 entrance window and a KBr-coated photocathode), which operates at 9.88 eV photon energy. Details of the spectrometer can be found in Refs. 22 and 23. The spectral sensitivity of the bandpass detector has been measured with synchrotron radiation and shows an asymmetric profile with a smooth onset on the low-energy side. The overall spectrometer function as obtained by a convolution of the detector sensitivity and the energy distribution of the electron source has a FWHM of 640 meV and can be used for numerical deconvolution of the spectra. The energy reference used here is given by the Fermi edge of a sputtered Au film measured under identical conditions as the samples.

Single crystals of $1T$-TaS_2 were prepared from the elements by the iodine-vapor-transport method. Detailed crystal-growth parameters are given in Ref. 6. The structure and quality of the samples was controlled by x-ray diffraction and by temperature-dependent measurement of the electrical resistivity. Clean surfaces were obtained by cleavage perpendicular to the c axis under ultrahigh-vacuum conditions in the low 10^{10}-mbar range. The surface quality was checked by STM and low-energy electron diffraction (LEED). In particular, we performed temperature-dependent LEED in the range 130–400 K. The CDW is observed as fractional-order spots in the LEED pattern. At room temperature the superlattice spots are found to be rotated with respect to the underlying 1×1 structure by $11.7°\pm0.5°$. At 350 K we observe a sudden drop of the tilt angle to 0° within 5 K, coinciding with the $1T_2$-to-$1T_1$ transition temperature observed in resistivity. Upon cooling from room temperature, the rotation angle gradually increases until it saturates for temperatures below about 200 K at about $13.5°\pm0.5°$. A LEED pattern taken at 130 K with the crystal in the low-temperature phase is shown in Fig. 3. The measured rotation angles are in good agreement with the work of Scruby *et al.*,[15] and the observed coincidence of bulk and surface transitions confirms the result of Ref. 18.

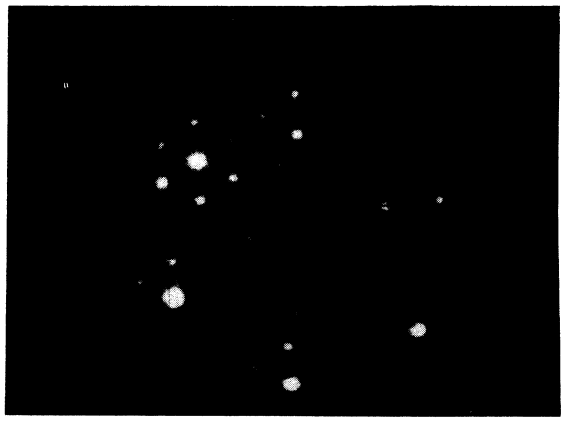

FIG. 3. LEED pattern of a cleaved (0001) surface of $1T$-TaS_2 at 130 K, $E_p = 92$ eV.

The work function (vacuum level minus Fermi level) necessary to determine the wave vector from the energy and incidence angle of the impinging electron in ARIPES has been determined by target-current spectroscopy (TCS) to be about 5.7 eV for a freshly cleaved surface. The method has been described previously.[24] Work-function measurement by TCS has also been utilized to monitor surface cleanliness during ARIPES, since the same electron source was used. Though at room temperature the surface was found to be stable over a period of weeks, during the low-temperature measurements the work function dropped as low as 4.7 eV within a few days as a result of surface contamination.

Azimuthal orientation of the samples necessary for the angle-resolved work was performed by LEED and x-ray diffraction (Laue method). In order to distinguish between the nonequivalent ΓALM and $\Gamma AL'M'$ half-planes (cf. Fig. 1), we calculated Laue patterns and compared them to the measured diffraction patterns.

IV. ARIPES AT ROOM TEMPERATURE

We have performed angle-resolved inverse photoemission spectroscopy at room temperature along the high-symmetry directions ΓM, $\Gamma M'$, and ΓK of the Brillouin zone of the disordered $1T$ structure. The spectra are shown in Fig. 4 for various angles of electron incidence.

At first sight, we find in nearly all spectra two distinct structures centered at about 1 and 4 eV above the Fermi level, which can clearly be attributed to the t_{2g} and e_g manifolds, respectively. Also, we observe a marked difference in intensity between the ΓM and $\Gamma M'$ spectra. Due to the disappearance of the e_g bands along the ΓM direction, a further peak at about 6 eV becomes visible, traces of which are also to be seen in the $\Gamma M'$ and ΓK spectra.

The t_{2g} and e_g emissions reveal a distinct substructure, which can be clearly traced when the angle of electron incidence, ϑ, is varied. In order to resolve this substructure, we performed a detailed evaluation of the spectra by deconvolution with the known spectrometer function and a subsequent numerical fitting procedure. Great care has been taken to avoid numerical artifacts by considering the results only reliable when a stable convergence was achieved, and the structures obtained in this way were already visible in the original spectra. The resulting peak positions are indicated as tic marks in Fig. 4; added solid circles denote the dominant emission within each manifold. By applying the standard interpretation of ARIPES, these results were converted into an experimental conduction-band structure $E(k_{\parallel})$, which is displayed in Fig. 5. For comparison, also the band-structure calcu-

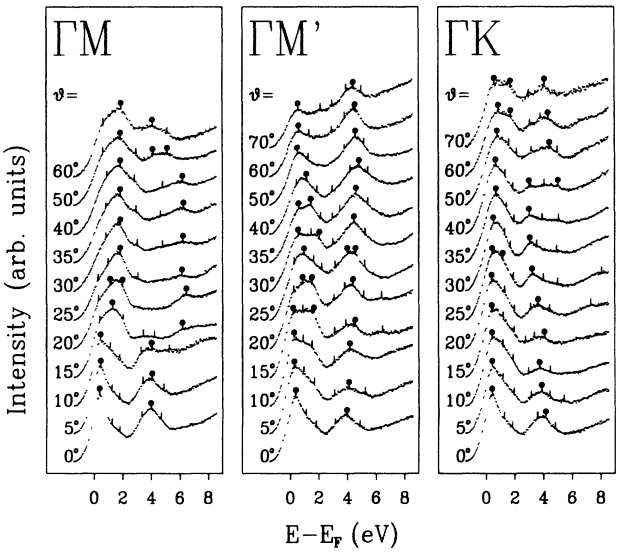

FIG. 4. Angle-resolved inverse photoemission spectra at room temperature along the high-symmetry directions ΓM, $\Gamma M'$, and ΓK for various angles of incidence. Peak positions are denoted by tic marks, strong emissions by solid circles.

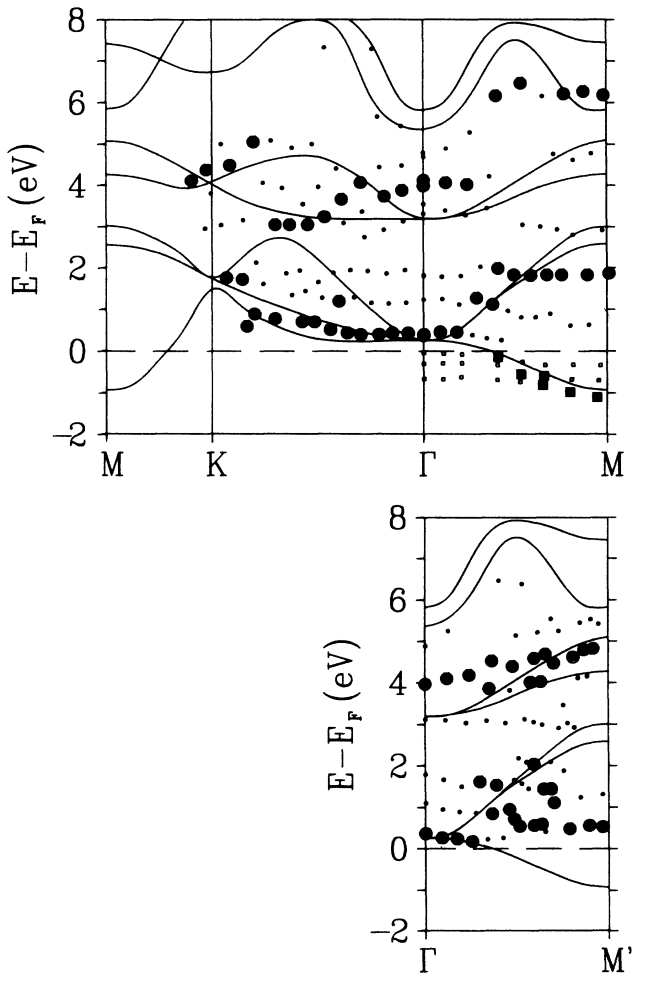

FIG. 5. Experimental room-temperature conduction-band structure compared to the calculation of Mattheiss (Ref. 11). Upper panel contains data obtained along ΓM and ΓK, lower panel along $\Gamma M'$. The upper panel also contains ARPES results (squares) of Ref. 6. Strong emissions are indicated by large symbols.

lation of Mattheiss[11] for the undistorted $1T$ structure is included, which already contains all important features also present in subsequent calculations.[9,12] Despite some experimental uncertainty of the normal component of the electron momentum, $k_\perp$, we show for reasons of clarity the theoretical bands only for the basal (ΓKM) plane of the Brillouin zone. This seems reasonable since the theoretical $k_\perp$ dispersions of the Ta $5d$ bands are generally smaller than 0.4 eV and will not be of major importance in the following discussion. Also, we will further on refer to the measured directions as ΓM, $\Gamma M'$, and ΓK, though, strictly speaking, the electron wave vector lies in the ΓALM, $\Gamma AL'M'$, and ΓAHK half-planes, respectively.

In the analysis of the data very good convergence for the t_{2g} emission was obtained when it was fitted with three Gaussians, each displaying only little $k_\parallel$ dispersion (<500 meV). However, when following the main emission (indicated by solid circles in Figs. 4 and 5) of the t_{2g}-derived structure through varying values of ϑ, we find intensity exchange between the substructures. For instance, along the ΓK direction the center-of-gravity emission follows very closely the upward dispersion of the theoretically predicted d_{z^2}-derived band. Along ΓM the substructure which is strongest at $\vartheta=0°$ weakens for $\vartheta \geq 15°$, until it vanishes for angles greater than 25°. Instead, the main intensity shifts towards the emission at about 2 eV above E_F, similar to the dispersion of the theoretical $d_{x^2-y^2}/d_{xy}$-derived bands, which rise up to 3 eV above the Fermi energy. The disappearence of the lowest structure for higher angles of incidence can be interpreted as the crossing of the d_{z^2}-derived conduction band through the Fermi level. This interpretation is nicely confirmed by comparison to ARPES data of the occupied part of the d_{z^2} band,[6] which are included in the upper panel of Fig. 5. Like our inverse photoemission results, the ARPES spectra show a manifold of almost dispersionless states with intensity shifts occuring between them.[5,6] The combined ARPES and ARIPES results show that the main intensity very closely follows the d_{z^2}-derived conduction band of Mattheiss in both the occupied and unoccupied energy regimes, respectively. For the $\Gamma M'$ spectra the situation is less clear. The crossing of the lowest emission through E_F seems to appear in the same way as along ΓM, but we do not observe a conclusive behavior of the intensity shifts for the higher-lying t_{2g} emissions (lower panel of Fig. 5), though the spectra were reproducible for several samples. The overall width of the unoccupied part of the t_{2g} manifold using $\Gamma M'$ is about 2 eV, in complete agreement with the result obtained along ΓM and also along ΓK, but still 1 eV less than the theoretical prediction for the pure $1T$ phase.

The e_g manifold is most pronounced in the $\Gamma M'$ spectra. The center-of-gravity emission slowly disperses from 4 eV above E_F at Γ to about 5 eV at the M' point, but from the satellite emissions an overall bandwidth of about 2.5 eV can be estimated. The same result is obtained from the ΓK spectra. This is slightly larger than the value of 2 eV calculated by Mattheiss. As stated above, the e_g emission completely disappears for higher angles of incidence along ΓM, leaving room for a relatively weak structure at above 6 eV, which compares well with the calculated energies of the antibonding metal $6s$-$6p$-derived states. In our ARIPES spectra of $1T$-TaS_2 we did not find a candidate for an image-potential state as in other transition-metal dichalcogenides,[20,21,25,26] because the crucial requirement for such a state—an energy gap close below the vacuum level—is not met here since the e_g manifold is located in this energy range.

In summary, both the t_{2g} and e_g manifolds reveal a substructure of almost dispersionless states, while the locations of the dominant emission within each manifold seem to reflect the predicted dispersions of the undistorted $1T$ structure. This is very similar to the situation in ARPES, where the occupied part of the d_{z^2} band also splits into several submanifolds, but the position of the main emission closely follows the undistorted band dispersion.[5,6] It has been shown by Smith *et al.*,[5] by applying an empirical tight-binding scheme, that the splitting can be understood as a consequence of the CDW state. Due to the folding of bands into the smaller CDW Brillouin zone, additional band crossings occur, which are lifted by taking into account the CDW atomic displacements and their effect on the interband interactions. Thus, new energy gaps appear which separate the submanifolds from each other. Unfortunately, this calculation was only performed for energies up to 0.4 eV above the Fermi level. It seems reasonable to propose a similar effect also for the unoccupied Ta $5d$ bands, though the finite energy resolution in this experiment does not allow us to decide whether we have real energy gaps between the subpeaks or only a reduced density of states. These arguments apply only for the low-temperature CDW phase, but may be appropriately extended also to the room-temperature phase, if the commensurate domain model is valid.

It remains to be explained why the intensity shifts of the CDW system resemble so closely the band dispersions of the hypothetical $1T$ structure. While the CDW-derived superlattice is responsible for a rearrangement of the electronic states in **k** space, the overall shape of the electron wave functions is governed by the crystal potential of the $1T$ lattice, whose Fourier components are still considerably larger than the CDW-related contribution to the total potential. Thus, the dipole matrix elements describing the transition probability of the (inverse) photoemission process will only slightly be affected by the CDW, resulting in the observed intensity variations.

As mentioned above, we observe distinct intensity differences between the ΓM and $\Gamma M'$ spectra, reflecting the threefold symmetry of the crystal structure. This is most clearly seen in the almost complete vanishing of the e_g emission along the ΓM direction for $\vartheta \geq 15°$, while it is stronly pronounced in the $\Gamma M'$ spectra. On the other hand, the intensity of the t_{2g}-derived bands along $\Gamma M'$ for higher values of ϑ seems to be reduced compared to ΓM, which is possibly the reason for our inability to derive a conclusive dispersion behavior of the intensity variations in the $\Gamma M'$ spectra. Both effects have also been observed in all other transition-metal dichal-

cogenides possessing the $1T$ structure that we have studied with ARIPES so far [$1T$-$TiTe_2$ (Ref. 21), $1T$-TiS_2 (Ref. 25), and $1T$-VSe_2 (Ref. 26)]. A similar asymmetry concerning the d_{z^2} band of $1T$-TaS_2 occurs in the ARPES spectra of Smith and Traum,[3] where reduced photoemission intensity along $\Gamma M'$ was found, which the authors ascribe to the opaqueness of the adjacent sulfur atom for the escaping photoelectron. Such a shadowing effect does not suffice to explain our observations, because in that case the suppression of the e_g emission should be most pronounced for $\vartheta = 55°$, the angle between the Ta—S bond and the surface normal. The reduction of the t_{2g} intensity even occurs along the wrong direction, since the electron is incident from the ΓM direction (where the sulfur is located beneath the Ta plane), when the electron momentum is in the $\Gamma AL'M'$ half-plane. For a detailed understanding of the relationship between inverse photoemission intensity and geometry, an accurate calculation of the matrix elements describing the optical transition from the incident LEED wave into the Ta $5d$-derived bands is required, analogous to existing studies of the photoemission intensities.[27]

V. TEMPERATURE-DEPENDENT ARIPES

The conduction-band structure has also been investigated as function of the temperature. In particular, we were interested in changes below the $1T$-$1T_3$ transition at 180 K and whether the opening of the localization gap can be observed also in the unoccupied band structure. Therefore, we have recorded ARIPES spectra along the high-symmetry directions at $T = 120$ K. The overall impression obtained from the low-temperature data is that the band structure is hardly affected by the change in temperature. We find the same structures and intensity modulations as in the room-temperature experiments. Therefore, the spectra are not reproduced here. This observation may be well understood when assuming the commensurate domain model for the $1T_2$ phase. In this case we would expect essentially the same electronic structure below and above the phase transition, except that the features in the room-temperature spectra will be broadened in energy, due to the lack of phase coherence across the discommensurations separating the individual domains. This is exactly what has been observed in photoemission,[5,6] but when extrapolating the linewidths observed there (< 200 meV) to the unoccupied states such a broadening seems to be far below our experimental resolution.

We now focus on the conduction bands close to the Fermi level. In a recent high-resolution ($\Delta E = 35$ meV) angle-resolved photoemission experiment,[7] the occupied part of the d_{z^2}-derived band was found to shift away from the Fermi energy, leaving behind an energy gap of 200 meV referred to E_F. The interesting question now is whether a similar gap at E_F occurs in the unoccupied band structure. It would be natural to study a possible gapping at the crossing of the d_{z^2} band through E_F, i.e., directly on the Fermi surface. Unfortunately, it turns out to be extremely difficult to detect an effect of the order of 100 meV at a Fermi edge, whose spectral width is determined by our experimental energy resolution of 640 meV. Instead, the temperature-dependent energy position of the strongly developed d_{z^2} peak at about 0.5 eV for normal incidence was measured (cf. Fig. 4). We assume that a shift of this peak can be taken as a measure for an energy gap, if it occurs at all, because in photoemission the complete d_{z^2}-derived manifold was found to shift rigidly away from the Fermi level in line with the opening of the gap. A change of about 100 meV in peak position in the ARIPES spectra would thus be much easier to detect.

In Fig. 6 we show a selection of spectra for a cooling series from 300 to 120 K and a warming-up cycle from 120 to 400 K. Clearly, the temperature effect is very small. The peak positions have been determined after numerically smoothing the spectra in order to get rid of the statistical noise. The final results were found to be independent of the algorithms and parameters used in the smoothing procedure. Thus, effects due to the numerics can be excluded. The energy shift of the d_{z^2} peak with respect to its low-temperature position as function of the temperature is shown in Fig. 7. There is an obvious trend of the peak position to higher energies as the temperature is lowered, but we do not observe any drastic changes near the phase transitions. When taking a closer look at the data, one may perceive a small step at about 350 K and a slight hysteresis of the cooling and heating branches between ≈ 180 and ≈ 220 K. Both effects occur close to transition temperatures and have been seen in several samples, but since they are so small in size, compared to the experimental and statistical uncertainty indicated by the error bar in Fig. 7, we do not think it appropriate to draw definite conclusions from these obser-

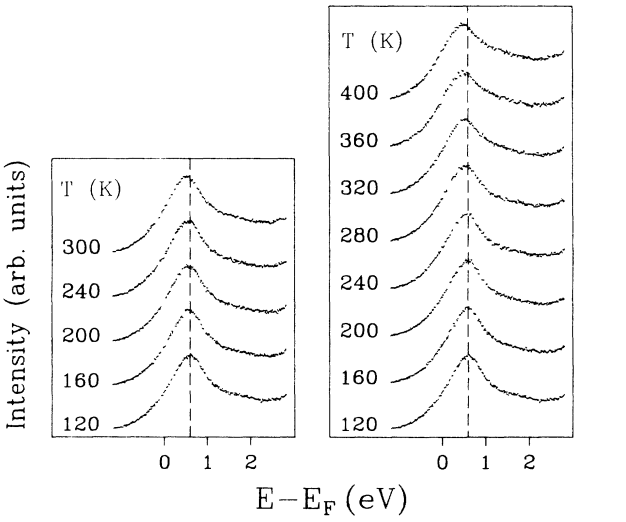

FIG. 6. Temperature-dependent ARIPES spectra of the d_{z^2} band at normal incidence. Left, cooling series; right, warming-up series. The dashed line marks the energy position of the d_{z^2} peak at 120 K. Note the shift to lower energies for increasing temperature.

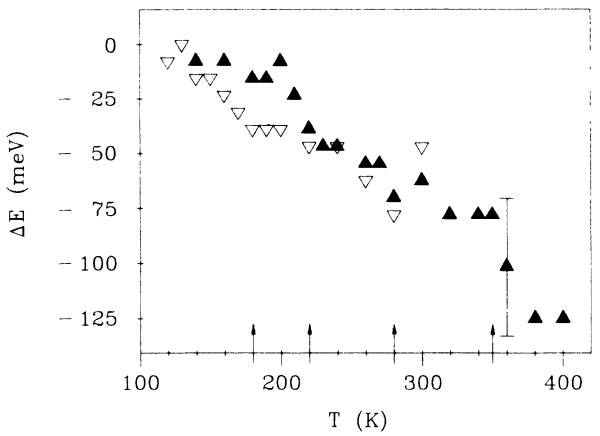

FIG. 7. Energy shift of the d_{z^2} emission with respect to its low-temperature position ($T=120$ K) as a function of temperature. Open and solid triangles denote data obtained from the cooling and heating cycles, respectively. The error bar indicates the estimated uncertainty. Arrows denote phase-transition temperatures.

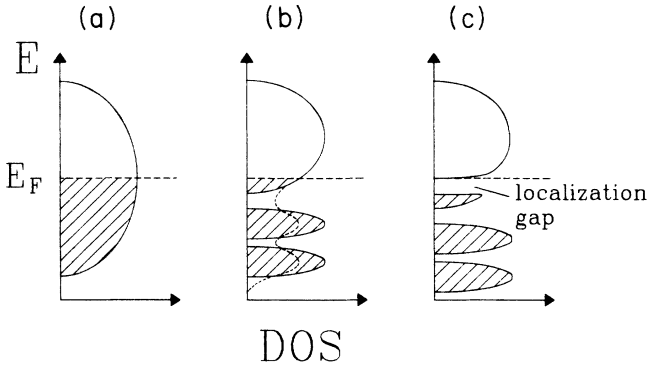

FIG. 8. (a) Density of states for the d_{z^2} band in the undistorted $1T$ phase. (b) Effect of the CDW on the conduction band as calculated in Ref. 5; the dashed curve denotes the effect of broadening (see text). (c) Opening of the localization gap and pinning of the Fermi level close to the lowest unoccupied band in the low-temperature phase.

vations concerning changes due to phase transitions. The overall temperature dependence of the energy of the d_{z^2}-derived conduction-band state at the Γ point is believed to be essentially determined by conventional electron-lattice interaction and can be fitted linearly to give a temperature coefficient of 0.35 meV/K, which is the order of magnitude observed in other metals and semiconductors (≈ 0.2 meV/K).[28]

What we can conclude from the temperature-dependent spectra is that, if there are any effects on the unoccupied electronic states due to the $1T_2$-$1T_3$ transitions, they must be considerably smaller than 100 meV, the order of magnitude of the gap in the occupied energy range. We may even conclude that the localization gap opens entirely in the occupied band structure, the Fermi level being pinned close to the lowest unoccupied states.

VI. QUALITATIVE MODEL OF THE TEMPERATURE-DEPENDENT ELECTRONIC STRUCTURE

From the combined results of ARPES and ARIPES and previous theoretical work on the electronic structure of $1T$-TaS_2, we finally try to derive a consistent picture of the electronic band structure near E_F in the CDW phases from combined ARPES and ARIPES results. Above all, it is interesting to focus on the d_{z^2}-derived conduction band in the vicinity of E_F, which determines the electrical properties of $1T$-TaS_2. For simplicity, here we shall discuss its behavior in terms of the density of states.

In the undistorted $1T$ state the d_{z^2} band has a width of about 2.5 eV, as predicted by Mattheiss, which agrees well with the intensity dispersions associated with this state in both the ARPES and ARIPES spectra (cf. Fig. 5). As indicated in Fig. 8(a), the band is half-filled, i.e., it contains 13 electrons if referred to the unit cell of the $\sqrt{13}\times\sqrt{13}$ reconstruction. The effects of the CDW on this band have been studied in detail by Smith *et al.*[5] for the case of the low-temperature phase. In their calculation the d_{z^2} band splits into three submanifolds, separated by gaps of 100 and 200 meV, respectively, which is depicted in Fig. 8(b). The lower two subbands are filled with six electrons each; the upper one is only partly filled, containing the thirteenth electron. Thus, the conduction-electron density becomes strongly reduced. However, assuming the commensurate domain model for the $1T_2$ phase, we expect a broadening of these bands due to phase scattering between the domains, which can be observed in photoemission. Now it seems likely that the broadening is sufficient to result in overlap between the subbands, hence restoring the original conduction-electron density. This behavior is indicated by the dashed line in Fig. 8(b).

As we go through the $1T_2$-$1T_3$ phase transition, the overlap drops to zero and the thirteenth electron becomes separated from the rest of the d_{z^2} manifold as in the original result of Smith *et al.* The remaining carrier density is drastically reduced by a factor of 13 and fails to provide sufficient metallic screening, making the conduction electrons susceptible to a Mott localization, which was first suggested by Fazekas and Tosatti.[8] The photoemission and inverse photoemission data, together, indicate that the corresponding localization gap opens only in the occupied band structure, leaving the empty electronic states unaffected [Fig. 8(c)]. Thus, the absolute size of the gap is already given by the 200-meV shift of the occupied part of the d_{z^2} band observed in ARPES.[7]

In order to explain why the location of the Fermi level appears to be fixed close to the lowest unoccupied band at the low-temperature transition, it may be useful here to adopt a semiconductor-like description. It is known from the semiconducting transition-metal dichalcogenides that they can be n-type doped due to the tendency of self-intercalation of the transition metal [e.g., TiS_2 (Ref. 29)]. It seems possible that additional electrons from excess Ta atoms in the van der Waals gaps are able to populate the

bottom of the upper subband, creating a situation as in a degenerate semiconductor. In this case the localization gap would indeed occur completely in the occupied band structure, but then one would expect to see traces of the upper band in photoemission, unless the density of states as its bottom is beyond the detection limit. Since the ARPES results have not supported such an explanation as yet, we are led to consider also a pinning of the Fermi level to donor levels close below the lowest unoccupied states as in a nondegenerate semiconductor. We have to favor the latter pinning situation as long as no Fermi-edge emission is seen in photoemission.

VII. CONCLUSIONS

In this work we have investigated the effects of the CDW on the unoccupied electronic structure of $1T$-TaS_2 by angle-resolved inverse photoemission. We could clearly identify the t_{2g}- and e_g-derived manifolds, which themselves reveal a substructure of almost nondispersing bands. The intensity modulations within the substructure are found to follow closely the calculated band dispersions of the undistorted $1T$ structure. The experimental conduction-band structure is explained by folding of bands into the smaller CDW-related Brillouin zone and additional interband interactions, similar to the interpretation of corresponding ARPES data. The observed intensity modulations indicate that the dipole matrix elements are only slightly affected by the CDW. Large asymmetries are found in the Ta $5d$-derived emissions between the ΓM and $\Gamma M'$ spectra, which cannot be explained by a shadowing effect of the chalcogen atoms.

Temperature-dependent measurements revealed no discontinuos changes of the unoccupied electronic structure at the low-temperature phase transition. In particular, we found no indication for the opening of a localization gap above the Fermi level as has been observed in the occupied band structure. Instead, the Fermi level is found to be pinned close to the bottom of the lowest unoccupied band, similar to the situation in a strongly doped n-type semiconductor. The absolute size of the localization gap is thus already determined by the 200-meV shift of the occupied part of the d_{z^2}-derived band observed in ARPES. From the combination of photoemission and inverse photoemission results, we derived a qualitative model of the temperature dependence of the conduction-band structure, considering the effects of CDW formation. Mott localization, and possible n-type doping. We hope that our results will encourage theorists to pursue a more elaborate and quantitative analysis of the still fascinating electronic properties of $1T$-TaS_2.

ACKNOWLEDGMENTS

We are grateful to Professor W. Schattke and his group for many helpful discussions on the electronic properties of layered materials. We would also like to thank W. Krüger for growing the crystals and L. Baumgarten for providing the STM pictures of the samples. This work was supported by the Deutsche Forschungsgemeinschaft (Bonn, Germany) under Project No. Sk-13/4.

[1]J. A. Wilson, F. J. DiSalvo, and S. Mahajan, Phys. Rev. Lett. **32**, 882 (1974).
[2]J. A. Wilson, F. J. DiSalvo, and S. Mahajan, Adv. Phys. **24**, 117 (1975).
[3]N. V. Smith and M. M. Traum, Phys. Rev. B **11**, 2087 (1975).
[4]R. A. Pollak, D. E. Eastman, F. J. Himpsel, P. Heimann, and B. Reihl, Phys. Rev. B **24**, 7435 (1981).
[5]N. V. Smith, S. D. Kevan, and F. J. DiSalvo, J. Phys. C **18**, 3175 (1985).
[6]R. Manzke, O. Anderson, and M. Skibowski, J. Phys. C **21**, 2399 (1988).
[7]R. Manzke, T. Buslaps, B. Pfalzgraf, M. Skibowski, and O. Anderson, Europhys. Lett. **8**, 195 (1989).
[8]P. Fazekas and E. Tosatti, Physica B + C (Amsterdam) **99B**, 183 (1980).
[9]A. M. Woolley and G. Wexler, J. Phys. C **10**, 2601 (1977).
[10]J. A. Wilson and A. D. Yoffe, Adv. Phys. **18**, 193 (1969).
[11]L. F. Mattheiss, Phys. Rev. B **8**, 3719 (1973).
[12]H. W. Myron and A. J. Freeman, Phys. Rev. B **11**, 2735 (1975).
[13]R. L. Withers and J. A. Wilson, J. Phys. C **19**, 4809 (1986).
[14]R. Brouwer and F. Jellinek, Physica B + C (Amsterdam) **99B**, 51 (1980).
[15]C. B. Scruby, P. M. Williams, and G. S. Parry, Philos. Mag. **31**, 255 (1975).
[16]W. L. McMillan, Phys. Rev. B **14**, 1496 (1976); K. Nakanishi and H. Shiba, J. Phys. Soc. Jpn. **53**, 1103 (1984).
[17]X. L. Wu and C. M. Lieber, Science **243**, 1703 (1989).
[18]R. E. Thomson, U. Walter, E. Ganz, J. Clarke, A. Zettl, P. Rauch, and F. J. DiSalvo, Phys. Rev. B **38**, 10 734 (1988).
[19]N. V. Smith, Rep. Prog. Phys. **51**, 1227 (1988).
[20]W. Drube, I. Schäfer, G. Karschnick, and M. Skibowski, Phys. Rev. B **30**, 6248 (1984).
[21]W. Drube, I. Schäfer, and M. Skibowski, J. Phys. C **20**, 4201 (1987).
[22]N. Babbe, W. Drube, I. Schäfer, and M. Skibowski, J. Phys. E **18**, 158 (1985).
[23]I. Schäfer, W. Drube, M. Schlüter, G. Plagemann, and M. Skibowski, Rev. Sci. Instrum. **58**, 710 (1987).
[24]R. Claessen, H. Carstensen, and M. Skibowski, Phys. Rev. B **38**, 12 582 (1988).
[25]R. Claessen (unpublished).
[26]I. Schäfer, doctoral thesis, University of Kiel, 1986.
[27]A. Liebsch, Solid State Commun. **19**, 1193 (1976).
[28]P. B. Allen and V. Heine, J. Phys. C **9**, 2305 (1976).
[29]C. H. Chen, W. Fabian, F. C. Brown, K. C. Woo, B. Davies, B. DeLong, and A. H. Thompson, Phys. Rev. B **21**, 615 (1980).

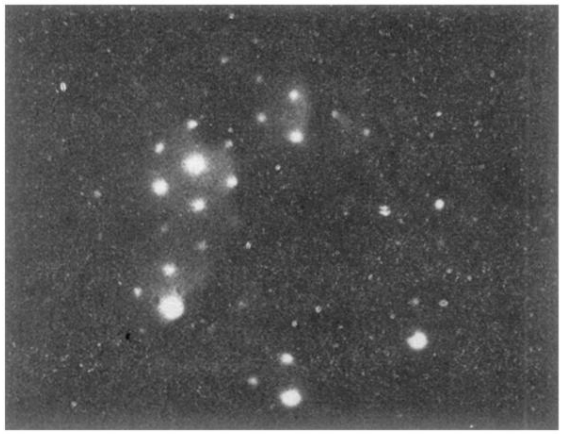

FIG. 3. LEED pattern of a cleaved (0001) surface of $1T$-TaS_2 at 130 K, $E_p = 92$ eV.